Journal of Systems Engineering and Electronics
Vol. 34, No. 1, February 2023, pp.224 – 235

Flexible predictive power-split control for battery-supercapacitor systems of electric vehicles using IVHS

HE Defeng[1,*], LUO Jie[1], LIN Di[2], and YU Shiming[1]

1. College of Information Engineering, Zhejiang University of Technology, Hangzhou 310023, China;
2. BYD Company Limited, Huizhou 516083, China

Abstract: The utilization of traffic information received from intelligent vehicle highway systems (IVHS) to plan velocity and split output power for multi-source vehicles is currently a research hotspot. However, it is an open issue to plan vehicle velocity and distribute output power between different supply units simultaneously due to the strongly coupling characteristic of the velocity planning and the power distribution. To address this issue, a flexible predictive power-split control strategy based on IVHS is proposed for electric vehicles (EVs) equipped with battery-supercapacitor system (BSS). Unlike hierarchical strategies to plan vehicle velocity and distribute output power separately, a monolayer model predictive control (MPC) method is employed to optimize them online at the same time. Firstly, a flexible velocity planning strategy is designed based on the signal phase and time (SPAT) information received from IVHS and then the Pontryagin's minimum principle (PMP) is adopted to formulate the optimal control problem of the BSS. Then, the flexible velocity planning strategy and the optimal control problem of BSS are embedded into an MPC framework, which is online solved using the shooting method in a fashion of receding horizon. Simulation results verify that the proposed strategy achieves a superior performance compared with the hierarchical strategy in terms of transportation efficiency, battery capacity loss, energy consumption and computation time.

Keywords: electric vehicle (EV), model predictive control (MPC), Pontryagin's minimum principle (PMP), power-split.

DOI: 10.23919/JSEE.2023.000013

1. Introduction

With the rapid development of urban modernization, the issues of fuel consumption and exhaust emissions of transportation systems have drawn increasing attention [1]. Vehicle electrification, such as hybrid electric vehicle (HEV), plug-in hybrid electric vehicle (PHEV) and electric vehicle (EV), has been viewed to be a key way to address these issues. Among them, EV is the most promising alternative due to the features of regenerative braking and zero emissions [2]. However, the pressures of insufficient power density and capacity loss for battery are still the primary restrictions for wide production and application of EVs [3,4]. To relieve these pressures, a battery-supercapacitor system (BSS) is generally used to be the supply unit of EV [5,6] and its superior performance compared with the battery-only powertrain has been verified in [7]. Meanwhile, to fully exploit the potential of BSSs, an efficient power-split strategy is required to distribute output power between the battery and the supercapacitor in real time [8]. The power-split strategies can be roughly divided into three categories: rule-based method [9], optimization-based method [10] and learning-based method [11]. The recent results on power-split strategies were summarized in [12].

Furthermore, the utilization of the traffic information received from intelligent vehicle highway system (IVHS) to plan the near future velocity trajectory cannot only effectively enhance the performance of EVs, but also shorten the travel time [13,14]. Due to the strongly coupling characteristic of the velocity planning and the power distribution, the hierarchical control architecture is generally used to address them separately. The higher-level controller plans the vehicle velocity trajectory using the traffic information to minimize the travel time, ensure ride comfort and avoid collision. And the lower-level controller distributes output power between different supply units according to the velocity trajectory obtained from the higher-level controller for minimizing fuel consumption and battery capacity loss [15–20]. Meanwhile, Sangjae et al. [21] showed that the vehicle performance can be further improved if special information is adopted, e.g., the traffic lights in urban roads [22]. Thus, Yuan et al. [23] designed a velocity predictor utilizing the histori-

Manuscript received January 27, 2022.
*Corresponding author.
This work was supported by the National Natural Science Foundation of China (62173303), and the Fundamental Research for the Zhejiang Provincial Universities (RF-C2020003).

cal signal phase and time (SPAT) information and the driver's intention, and then a power-split strategy for connected hybrid EVs (CHEVs) was proposed to distribute the output power between engine and battery based on the predicted velocity trajectory obtained from the velocity predictor. To coordinate the distinct energy consumption characteristics between EVs and traditional gasoline vehicles in a mixed-traffic platoon, He et al. [24] developed an eco-driving strategy to guide the mixed-traffic platoon in order to get through each intersection combining the upcoming SPAT information and the energy consumption characteristics of EVs and traditional gasoline vehicles, which improved transportation efficiency and energy efficiency.

It is well-known that it is necessary to plan the velocity trajectory online and distribute output power of EVs in a complex traffic environment. Model predictive control (MPC) is widely used to address these issues of EVs due to its ability to explicitly deal with system constraints and multi-objective optimization problems in real-time [25–28]. In [29], the MPC framework was adopted to optimize the velocity trajectory online of CHEVs in urban roads based on the SPAT information received from IVHS, and then an adaptive equivalent consumption minimization strategy (ECMS) was used to track the optimal velocity trajectory. More MPC-based power-split strategies were summarized in [30].

Although using the upcoming SPAT information transmitted from IVHS to plan velocity trajectory of CHEVs can improve the performance of the power-split strategy, there is lack of related efforts on connected EV equipped with BSS (CEV-BSS). Note that the power-split problem of CEV-BSS is not directly followed from the CHEVs', since the CEV-BSS and CHEVs are equipped with distinct supply systems and the power-split strategies pursue different optimization objectives [31,32]. In addition, the velocity planning and the power distribution are generally decoupled into two sub-problems and a hierarchical method is used to solve them separately in previous results [33]. However, the report from U.S. Department of Energy indicates that the vehicle performance can be improved significantly if the velocity planning and the power distribution can be addressed simultaneously [34].

Inspired by these previous works, in this paper a flexible receding horizon power-split strategy for CEV-BSS in urban roads is proposed to improve transportation efficiency, reduce energy consumption and relieve battery degeneration. The problems of velocity planning and power distribution are formulated as a flexible velocity planning strategy and an optimal control problem, respectively, and a monolayer MPC method is used to optimize them online simultaneously. Firstly, a flexible velocity planning strategy is designed based on the upcoming SPAT information, which guarantees that the CEV-BSS can get through each intersection without shutdowns. Meanwhile, the Pontryagin's minimum principle (PMP) is adopted to establish the optimal control problem of the BSS. Subsequently, the flexible velocity planning strategy and the optimal control problem are embedded into an MPC framework which is solved by the shooting method in a fashion of receding horizon. Moreover, to avoid the deterioration of ride comfort, the L_1 regularization regarded as the penalty of the objective function is introduced to trade off the flexibility and smoothness of vehicle velocities. Note that the time delays caused by information transmission will not be considered in this paper, because they could be generally compensated by shortening the duration of green light. Finally, several simulations are used to verify the effectiveness of the proposed strategy.

The main contributions of this paper are summarized as follows: (i) Unlike the hierarchical method to optimize the velocity trajectory and distribute output power between different supply units separately, a monolayer MPC is used to optimize them simultaneously in this paper. The simulation results validate the superiority of the proposed strategy compared with the hierarchical method in terms of traffic efficiency, battery life-time and adaptive ability to unknown scenarios. (ii) The flexible velocity planning strategy is designed based on the SPAT information to provide an extra degree of freedom for the power-split strategy. Meanwhile, the L_1 regularization is introduced to constrain the flexibility of vehicle velocity and then avoid the deterioration of ride comfort.

The rest of this paper is organized as follows. Section 2 builds the control-oriented models. The flexible predictive power-split control strategy is structured in Section 3. The simulation results are discussed in Section 4 and Section 5 concludes the paper.

2. Control-oriented models

This paper considers a CEV-BSS to get through N intersections with signal lights on a flat urban road, which is shown as Fig. 1. It is assumed that the CEV-BSS can receive the SPAT information from the signal lights of the downstream intersection through IVHS.

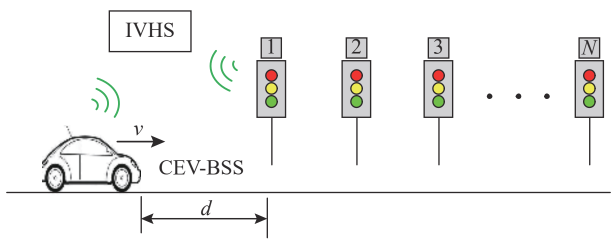

Fig. 1 A schematic of the traffic scenario

The longitudinal dynamics of vehicles composed of motor, rolling resistance, aerodynamic drag and gravitational force is considered in this paper. To trade-off accuracy and conciseness, it is assumed that the CEV-BSS runs on a flat and dry-asphalt road and ignores tire slip in the longitudinal direction. Thus, the vehicle longitudinal dynamics of CEV-BSS [35] can be described by

$$\begin{cases} \dot{s} = v \\ \dot{v} = u/m - gC_r - 0.5\rho C_d A v^2/m \end{cases} \tag{1}$$

where s, v and u denote the position, velocity and tractive force of CEV-BSS, respectively; m, C_r, ρ, C_d and A are the mass, rolling resistance coefficient, air density, drag coefficient and front area of the CEV-BSS, respectively.

Here, the configuration of the CEV-BSS is simplified as a BSS, an electric motor and a powertrain shown as Fig. 2. As the main power supply unit, BSS provides electrical energy to the motor and recovers part of braking energy through the direct current-direct current (DC-DC) bus. Then the tractive force generated by motor transmits to the powertrain along the mechanical joint. The differential unit distributes the tractive force to the tires on either side. In Fig. 2, the BSS consists of a battery pack, a supercapacitor pack and a bidirectional DC-DC converter, where the supercapacitor pack is connected in parallel with the battery pack through the bi-directional DC-DC converter [9,10]. For simplified calculation, the bi-directional DC-DC converter is generally modeled as an equivalent coefficient η, which represents the efficiency of the DC-DC convertor.

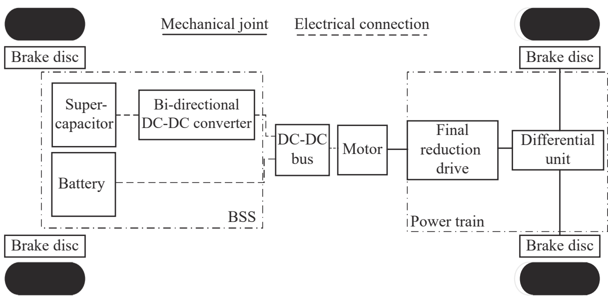

Fig. 2 Configuration of the CEV-BSS

The power flow between the BSS and the DC-DC bus [36] can be formulized as

$$\begin{cases} \eta P_{sc} = P_d - P_b \\ P_d = \left(m\dot{v} + mgC_r + 0.5\rho A C_d v^2\right) v \end{cases} \tag{2}$$

where P_d is the demanded power, P_b and P_{sc} are the output power of the battery and the supercapacitor, respectively.

In general, the high-fidelity models of batteries and supercapacitors cannot be applied in practice because of their complexity and the requirement of real-time applications. As shown in Fig. 3, the Rint/RC equivalent circuit consisted of a voltage source and an equivalent resistance in series is adopted in this paper.

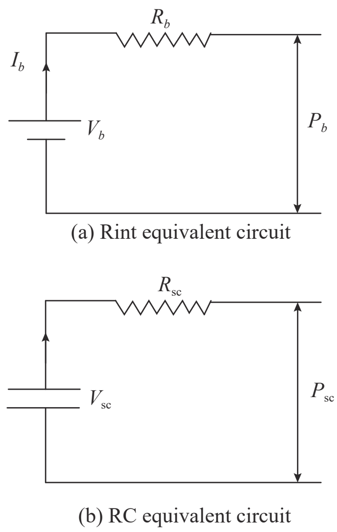

Fig. 3 Rint/RC equivalent circuit for the BSS

The dynamic characteristics of state of charge (SOC) for battery and supercapacitor [37] can be described as

$$\begin{cases} \dot{\mathrm{SOC}}_b = -\dfrac{I_b}{Q} = -\dfrac{V_b - \sqrt{V_b^2 - 4R_b P_b}}{2R_b Q} \\ \dot{\mathrm{SOC}}_{sc} = \dfrac{\sqrt{(\mathrm{SOC}_{sc} V_{sc,\max})^2 - 4R_{sc} P_{sc}}}{2R_{sc} C_{sc} V_{sc,\max}} - \dfrac{\mathrm{SOC}_{sc} V_{sc,\max}}{2R_{sc} C_{sc} V_{sc,\max}} \end{cases} \tag{3}$$

where SOC_b and SOC_{sc} represent the SOC of the battery and supercapacitor, respectively; Q, R_b, and V_b are the rated capacity, equivalent internal resistance and open circuit voltage of the battery pack, respectively; C_{sc}, R_{sc} and $V_{sc,\max}$ are the capacity, equivalent internal resistance and maximum rated voltage of the supercapacitor pack, respectively.

3. MPC-based flexible power-split

In this section, the flexible predictive power-split control strategy is proposed to plan velocity and distribute output power between battery and supercapacitor for CEV-BSS and avoid stopping at red lights to reduce travel time and minimize the output current of battery I_b, which improves energy efficiency and reduces battery capacity loss. As shown in Fig. 4, the proposed strategy roughly includes the following steps: (i) To avoid stopping at red lights, the velocity range that leads the CEV-BSS to cross the downstream intersection at green lights is calculated according to the SPAT information; (ii) For real-time computation requirement, the PMP is adopted to formulate the optimal control problem for CEV-BSS; (iii) Considering the velocity range and the optimal control problem, the flexible predictive power-split control strategy is designed with the shooting method.

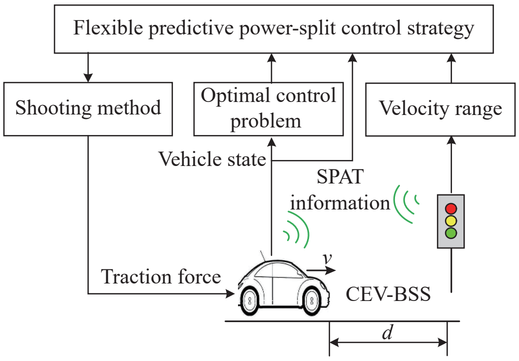

Fig. 4 A schematic of the proposed strategy

As described in Section 2, the CEV-BSS runs on a flat urban road with signal lights and it must observe the traffic rules. Apart from that, avoiding stopping at red lights can effectively reduce travel time. Thus, it is necessary to calculate the velocity range based on the SPAT information to guide the driving behaviors of the CEV-BSS. As shown in Fig. 5, t_s=t_r+t_g denotes the period of traffic light, where t_r and t_g are the duration of red light and green light, respectively; d represents the distance between the current positions of the CEV-BSS and downstream intersection.

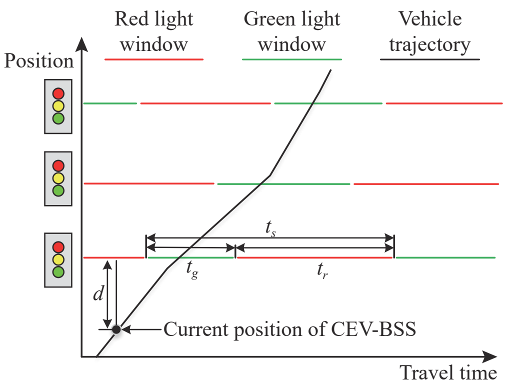

Fig. 5 A schematic of velocity range calculation

The velocity range at time instant t can be calculated as

$$v_h(t)=\begin{cases}\dfrac{d(t)}{Kt_s-t_g-t}, & \text{light}=\text{red}\\ v_{\max}, & \text{light}=\text{green}\,;\dfrac{d(t)}{Kt_s-t}\leqslant v_{\max}\\ \dfrac{d(t)}{Kt_s+t_r-t}, & \text{light}=\text{green and otherwise}\end{cases}, \tag{4}$$

$$v_l(t)=\begin{cases}\dfrac{d(t)}{Kt_s-t}, & \text{light}=\text{red}\\ \dfrac{d(t)}{Kt_s-t}, & \text{light}=\text{green};\dfrac{d(t)}{Kt_s-t}\leqslant v_{\max}\\ \dfrac{d(t)}{(K+1)t_s-t}, & \text{light}=\text{green and otherwise}\end{cases}, \tag{5}$$

$$\text{light}=\begin{cases}\text{red}, & 0\leqslant \bmod(t/t_s)\leqslant t_r\\ \text{green}, & t_r\leqslant \bmod(t/t_s)<t_s\end{cases}, \tag{6}$$

where $v_h(t)$ and $v_l(t)$ are the upper and lower bounds of the velocity, respectively, and K= ceil(t/t_s) is the number of traffic light cycle.

Due to its low computational complexity, PMP is usually used to solve large-scale optimization problems [38]. Combination of PMP and MPC can fully exploit their features of low computational burden and real-time applications. Thus, the PMP is adopted to formulate the optimal control problem for CEV-BSS, and then integrated into the MPC framework. Since the ampere-hour throughput takes the primary responsibility for the battery degradation and the internal resistance of the battery is greater than that of the supercapacitor, the performance of a power-split strategy can be evaluated by minimizing the battery current I_b [37]. Thus, the index function of power-split is formulated as

$$J_1=\alpha_1\int_{t_0}^{t_f} I_b^2(P_b,t)\mathrm{d}t \tag{7}$$

where α_1>0, t_0 and t_f are the weight, the initial time and the terminal time, respectively, and

$$I_b(P_b,t)=\left(V_b-\sqrt{V_b^2-4R_bP_b(t)}\right)/(2R_b).$$

Then, the dynamic characteristic of SOC for the supercapacitor is regarded as the state equation of the optimal control problem, which is

$$\dot{\mathrm{SOC}}_{\mathrm{sc}}(t)=f_1(\mathrm{SOC}_{\mathrm{sc}},P_{\mathrm{sc}},t). \tag{8}$$

Substituting (2) into (8), we can easily derive the coupling dynamic of the BSS that

$$f_1(\mathrm{SOC}_{\mathrm{sc}},P_{\mathrm{sc}},t)=f_1(\mathrm{SOC}_{\mathrm{sc}},u,P_b,t). \tag{9}$$

According to the PMP, the Hamiltonian function of the optimal control problem is defined as

$$H(\mathrm{SOC}_{\mathrm{sc}},u,P_b,\lambda,t)=\alpha_1 I_b^2(P_b,t)+\lambda(t)f_1(\mathrm{SOC}_{\mathrm{sc}},u,P_b,t) \tag{10}$$

where $\lambda(t)$ denotes the co-state variable corresponding to the coupling dynamics (9) of the BSS. The necessary conditions of the optimal control problem with respect to (7) are formulated as

$$\dot{\mathrm{SOC}}_{\mathrm{sc}}^*(t)=\frac{\partial H}{\partial\lambda}=f_1(\mathrm{SOC}_{\mathrm{sc}}^*,u^*,P_b^*,t), \tag{11}$$

$$\dot{\lambda}^*(t) = -\frac{\partial H}{\partial \mathrm{SOC_{sc}}} = -\lambda^*(t)\frac{\partial f_1(\mathrm{SOC_{sc}^*}, u^*, P_b^*, t)}{\partial \mathrm{SOC_{sc}}}, \quad (12)$$

$$H(\mathrm{SOC_{sc}^*}, u^*, P_b^*, \lambda^*, t) \leqslant H(\mathrm{SOC_{sc}^*}, u, P_b, \lambda^*, t). \quad (13)$$

Equations (11) and (12) guide the iterative direction of the state variable $\mathrm{SOC_{sc}}(t)$ and co-state variable $\lambda(t)$, and (13) guarantees that $u^*(t)$ and $P_b^*(t)$ can minimize the Hamiltonian function (10).

According to the velocity range (4)−(6) calculated above based on SPAT information and the optimal control problem (7)−(13) for the CEV-BSS, the flexible predictive power-split control strategy based on MPC is designed.

Let $\Delta t>0$ be the sampling time interval, N_p be the prediction horizon, vector $\boldsymbol{x}(i|k)$ denote the predicted variable at sampling time k for the future instant $k+i$. Define the state vector $\boldsymbol{x}=[\mathrm{SOC}_b, \mathrm{SOC_{sc}}, s, v, \lambda]^{\mathrm{T}}$ and output variable $y=I_b$. Combining (1)−(3) and (10)−(13), we have the interpolation function $f(\boldsymbol{x},u,P_b)=\boldsymbol{x}+\dot{\boldsymbol{x}}(u,P_b)\Delta t$ and the cost function

$$J(\boldsymbol{x}(k), u(k), P_b(k)) = \sum_{i=0}^{N_p-1}[H(\mathrm{SOC_{sc}}(i|k), u(i|k), P_b(i|k), \lambda(i+1|k), k) + \alpha_2\psi(i|k)] \quad (14)$$

where the L_1 regularization $\psi(i|k)=|v(i+1|k)-v(i|k)|$ for sparse outputs is introduced to avoid the deterioration of driving comfort, and α_2 is the weighted factor. Then the flexible predictive power-split control strategy is presented as

$$\begin{aligned}
&\min_{\substack{u(i|k)\\P_b(i|k)}} J(\boldsymbol{x}(k), u(k), P_b(k))\\
&\text{s.t. } \boldsymbol{x}(i+1\mid k) = f(\boldsymbol{x}(i\mid k), u(i\mid k), P_b(i\mid k))\\
&\quad y(i\mid k) = g(P_b(i\mid k))\\
&\quad \boldsymbol{x}_{\min} \leqslant \boldsymbol{x}(i\mid k) \leqslant \boldsymbol{x}_{\max}, P_{b,\min} \leqslant P_b(i\mid k) \leqslant P_{b,\max}\\
&\quad \begin{cases} u(i\mid k) = u_{\max}, & v(i\mid k) \leqslant v_l(i\mid k)\\ u(i\mid k) = u_{\min}, & v(i\mid k) \geqslant v_h(i\mid k)\\ u_{f,\min} \leqslant u(i\mid k) \leqslant u_{f,\max}, & \text{otherwise}\end{cases}\\
&\quad \left|\mathrm{SOC_{sc}^*}(N_p\mid k) - \mathrm{SOC_{sc,\,target}}(k)\right| \leqslant \zeta\\
&\quad \boldsymbol{x}(0\mid k) = \boldsymbol{x}(k), \quad i = 0, 1, \cdots, N_p-1
\end{aligned} \quad (15)$$

where the sequences $u(i|k)$ and $P_b(i|k)$ are the control variables, $\boldsymbol{x}_{\min}$ and $\boldsymbol{x}_{\max}$ are state constraints, $P_{b,\min}$, $P_{b,\max}$, $u_{\min}$, $u_{\max}$ are the physical limitation of power of battery and tractive force, respectively. $u_{f,\min}$ and $u_{f,\max}$ are the tractive force constraints associated with the velocity range $[v_L(k), v_h(k)]$, which ensure the avoidance of stopping at red lights. $\mathrm{SOC_{sc,target}}$ is the target SOC over the prediction horizon, which denotes the terminal constraint of the supercapacitor SOC. From (15), it can be observed that the CEV-BSS needs to catch up within $[v_l(k), v_h(k)]$ as much as possible.

The proposed strategy essentially results in a two-point boundary value problem to minimize (15) over the prediction horizon N_p. The shooting method is a typical approach to solve this problem for obtaining the numerical solution. The shooting method generally includes the following steps:

(i) Discretize the control variables over the prediction horizon, i.e.,

$$\begin{aligned}
&\boldsymbol{U}(k) = \begin{bmatrix} u(0|k) & u(1|k) & \cdots & u(N_p-1|k)\\ P_b(0|k) & P_b(1|k) & \cdots & P_b(N_p-1|k)\end{bmatrix},\\
&\Delta\boldsymbol{U} = \begin{bmatrix} u_{f,\max} - u_{f,\min}\\ P_{b,\max} - P_{b,\min}\end{bmatrix}/n_U,\\
&\begin{bmatrix} u(i|k)\\ P_b(i|k)\end{bmatrix} = \left(\begin{bmatrix} u_{f,\min}\\ P_{b,\min}\end{bmatrix} : \Delta\boldsymbol{U} : \begin{bmatrix} u_{f,\max}\\ P_{b,\max}\end{bmatrix}\right),\\
&i = 0, 1, \cdots, N_p-1,
\end{aligned} \quad (16)$$

where n_U determines the interval of the discretization of control variables.

(ii) Adjust the initial co-state variable $\lambda(0|k)$ of each shooting. The key step of the shooting method is adjusting the $\lambda(0|k)$ to hit a target state over the prediction horizon. Thus, a secant method [31,39] is employed to adjust the $\lambda(0|k)$ of each shooting, i.e.,

$$\begin{cases}
\lambda_1(0|k) = \lambda_0(0|k)\\
\lambda_2(0|k) = \lambda_0(0|k) + \delta\\
\lambda_q(0|k) = \lambda_{q-1}(0|k) - (\lambda_{q-1}(0|k) - \lambda_{q-2}(0|k))\cdot\\
\quad \left(\dfrac{\mathrm{SOC}_{\mathrm{sc},q-1}(N_p|k) - \mathrm{SOC_{sc,target}}(k)}{\mathrm{SOC}_{\mathrm{sc},q-1}(N_p|k) - \mathrm{SOC}_{\mathrm{sc},q-2}(N_p|k) + \alpha_3}\right)
\end{cases} \quad (17)$$

where $q=3, 4, \cdots, N_s$, N_s is a predetermined number of shooting points, and shooting interval $\delta = 0.04$, the coefficient α_3 ensures the denominator is nonzero. $\lambda_q(0|k)$ represents the initial co-state of the qth shooting at sampling instant k. $\mathrm{SOC}_{\mathrm{sc},q-1}(N_p|k)$ is the terminal SOC of the $(q-1)$ th shooting for supercapacitor at the instant k.

(iii) Minimize the objective function and guarantee that $\mathrm{SOC_{sc}^*}(N_p|k)$ converges to the target state $\mathrm{SOC_{sc,target}}(k)$, i.e.,

$$\begin{aligned}
&\boldsymbol{U}^*(k) = \arg\min_{U(k)} J(\boldsymbol{x}(k), u(k), P_b(k))\\
&\text{s.t. } \mathrm{SOC_{sc}^*}(i+1|k) = \mathrm{SOC_{sc}^*}(i|k) + \mathrm{SOC_{sc}^*}(i|k)\Delta t\\
&\quad \lambda_q^*(i+1|k) = \lambda_q^*(i|k) + \dot{\lambda}_q^*(i|k)\Delta t\\
&\quad |\mathrm{SOC_{sc}^*}(N_p|k) - \mathrm{SOC_{sc,target}}(k)| \leqslant \zeta
\end{aligned} \quad (18)$$

where $i=0, 1, \cdots, N_p-1$. As shown in Fig. 6, from the initial state $\mathrm{SOC_{sc}}(0|k_0)$, the target state $\mathrm{SOC_{sc,target}}(N_p|k_0)$ can be reached after n shots over the prediction horizon, where $0<n\leqslant N_s$. Then state $\mathrm{SOC_{sc}}(1|k_0)$ is viewed as the initial state $\mathrm{SOC_{sc}}(0|k_1)$ of next instant k_1. Repeat the shooting process until the actual state reaches the target state $\mathrm{SOC_{sc,target}}(k_f)$. The detailed pseudo-code is presented in Algorithm 1.

Algorithm 1 Pseudo-code for the power-split strategy

Initialization of parameters and variables
while $s(k)\leqslant s_{\max}$
  for $q = 1 : N_s$
    Generate the initial co-state variable using (17)
    for $i = 0 : N_p$
      for $i = 0 : N_p$
        Generate the target velocity range sequence (4)−(6)
    if $v_q(i|k) \leqslant v_l(i|k)$ or $v_q(i|k) \geqslant v_h(i|k)$
      if $v_q(i|k) \leqslant v_l(i|k)$
      $u_q^*(i|k) = u_{\max}$
      else if
      $u_q^*(i|k) = u_{\min}$
        Determine the optimal battery output power
      $P_b^*(k) = \arg\min\limits_{P_b(k)} J(\mathrm{SOC}_{\mathrm{sc}}^*, P_b, u^*, \lambda^*, k)$
        else
$$\Delta \boldsymbol{U} = \begin{bmatrix} u_{f,\max} - u_{f,\min} \\ P_{b,\max} - P_{b,\min} \end{bmatrix} / n_U$$
$$\begin{bmatrix} u(i|k) \\ P_b(i|k) \end{bmatrix} = \left(\begin{bmatrix} u_{f,\min} \\ P_{b,\min} \end{bmatrix} : \Delta \boldsymbol{U} : \begin{bmatrix} u_{f,\max} \\ P_{b,\max} \end{bmatrix} \right)$$
      for $z = 1 : n_U + 1$
        Determine the optimal input sequence by minimizing (8)
  $\boldsymbol{U}^*(k) = \arg\min\limits_{U(k)} J(x(k), u(k), P_b(k))$
        end
      end
    end
  if $|\mathrm{SOC_{sc}}(N_p|k)-\mathrm{SOC_{sc,target}}(k)|\leqslant\zeta$, break
end
Apply the first element of $\boldsymbol{U}^*(k)$ to CEV-BSS
$\boldsymbol{x}(k+1) = f(\boldsymbol{x}(k), u(0|k), P_b(0|k))$, $y(k)=g(P_b(0|k))$
Let $k=k+1$
end

Remark 1 It should be emphasized that this work focuses on the design of flexible predictive power-split control for BSSs of EV and presents a monolayer MPC method for the flexible predictive power-split control of the EV. Although the stability and feasibility issues of MPC are important, to the best of our knowledge, the theoretical result on the stability and feasibility problem of PMP-based nonlinear MPC is still an open and challenging issue. Note that the result on the solution convergence of PMP-based linear MPC can be found in [38]. Nevertheless, in practice one known method to guarantee stability of MPC is to impose the terminal constraint into the finite horizon optimization problem (15) with the heuristic method of tuning controller's parameters.

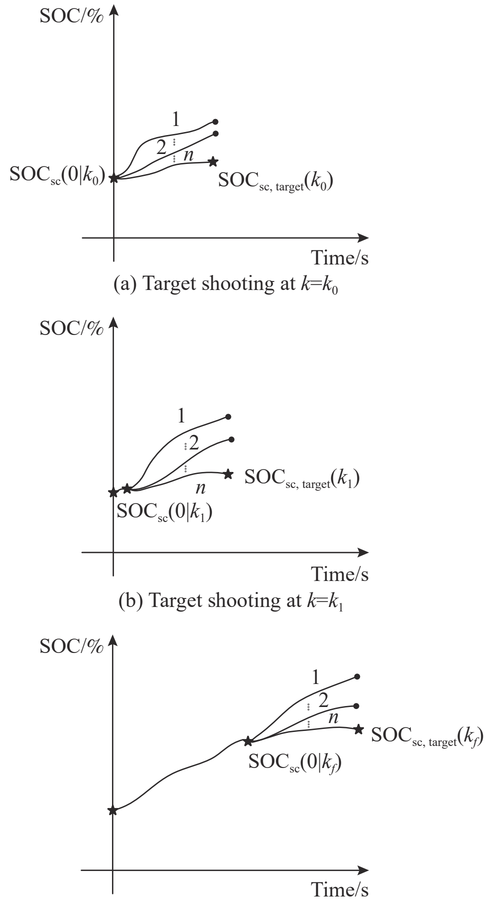

(a) Target shooting at $k=k_0$

(b) Target shooting at $k=k_1$

(c) Target shooting at $k=k_f$

Fig. 6 A schematic of the shooting method

Remark 2 The main idea of the strategy proposed in this work is to consider the traffic light information at intersections, calculate the speed range to avoid stopping and then provide a sparse velocity for CEV-BSS. The gently uniform speed can be calculated with L_1 regularization term according to the determined speed range, which can minimize the battery current throughput and then ensure satisfactory ride comfort during crossing the intersection.

4. Simulation results

In this section, the effectiveness of the proposed method is validated using the scenario of the real world of Hangzhou, China collected from Alimap. To demonstrate the superiority of the proposed strategy, the proposed method and a hierarchical MPC method [29] are compared under the urban road scenarios in [29]. Parameters of EV, battery pack and supercapacitor pack are listed in Table 1 and Table 2 [31], respectively. Simulation parameters are presented in Table 3.

Table 1 Parameters for the longitudinal dynamics

Parameter	Value
m/kg	1 550
ρ/(kg·m^{-3})	1.23
A/m^2	2.68
C_r	0.014
C_d	0.275

Table 2 Parameters of the BSS

Component	Parameter	Value
Battery pack	V_b/V	312
	Q/Ah	90
	R_b/Ω	0.3
Supercapacitor pack	$V_{\mathrm{sc,max}}$/V	310
	C_{sc}/F	2 500
	R_{sc}/Ω	0.01

Table 3 Simulation parameters

Parameter	Value	Parameter	Value
($u_{\min}$/$u_{\max}$)/N	3 100	($v_{\min}$/$v_{\max}$)/(m·s^{-1})	0/22
($\mathrm{SOC}_{b,\min}$/$\mathrm{SOC}_{b,\max}$)/%	20/100	$\mathrm{SOC}_{\mathrm{sc,ref}}$/%	75
($P_{b,\min}$/$P_{b,\max}$)/kW	−20/35	λ_0	0.1
($\mathrm{SOC}_{\mathrm{sc,min}}$/$\mathrm{SOC}_{\mathrm{sc,max}}$)/%	50/100	N_p	20
($P_{\mathrm{sc,min}}$/$P_{\mathrm{sc,max}}$)/kW	−105/105	N_s	10
ζ	0.001	Δt	1

4.1 Simulation results

The overview of Hangzhou, China is shown in Fig. 7, which has an approximate length of 2 200 m and includes six traffic lights. The initial speed, SOC_b and $\mathrm{SOC}_{\mathrm{sc}}$ of CEV-BSS are set as 6 m·s^{-1}, 90% and 75%, respectively. More details of the SPAT information for simulation are presented in Table 4, where the 'r-26' means that the signal light will turn from red to green after 26 s when the vehicles firstly enter the starting point. As shown in Fig. 8(a), the red/white interval indicates the duration of the red/green light, which means an impassable/accessible area, and the blue curve represents the driving route of the CEV-BSS. It can be observed that the proposed strategy enables the CEV-BSS to get through each intersection during green light.

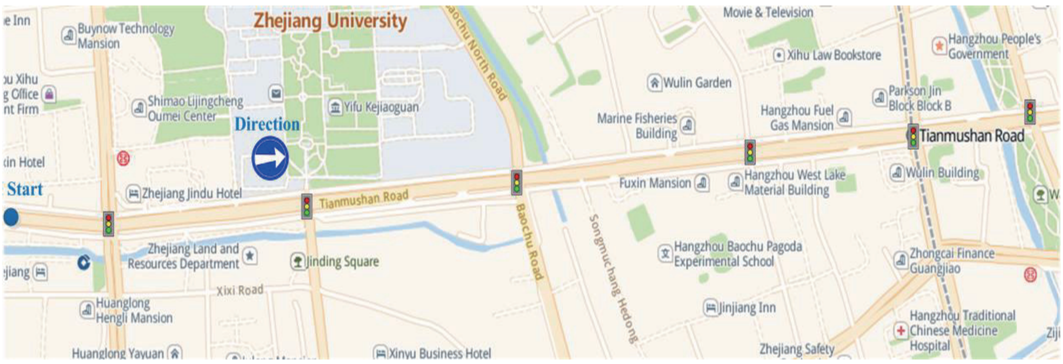

Fig. 7 Overview of Hangzhou, China collected from AMAP

Table 4 Details of SPAT information

Signal light	Initial state/s	Interval (t_r/t_g)/s	Distance/m
1st	r-26	45/20	210
2nd	g-2	40/25	428
3rd	g-18	45/20	460
4th	g-3	20/45	490
5th	g-6	40/25	357
6th	r-24	45/20	255

Meanwhile, the velocity trajectory of CEV-BSS in Fig. 8(b) indicates that the CEV- BSS can achieve a gentle driving behavior throughout the trip without shutdown. These can effectively improve transportation and energy efficiency since stop-and-go traffic is one of the main factors that cause traffic jams and additional energy consumption in urban roads. In addition, the power-split results of the proposed strategy are presented in Fig. 9, where the blue curve represents the demanded power for CEV-BSS and the red/green curve is the output power of battery/supercapacitor. It can be observed that the proposed strategy takes the ability to keep the output power of battery at a low level, and the supercapacitor is utilized to timely compensate the high-frequency demand power, which is beneficial to reduce battery capacity loss. Fig. 9 shows that the proposed strategy can ensure that the output powers of BSS meet the constraints.

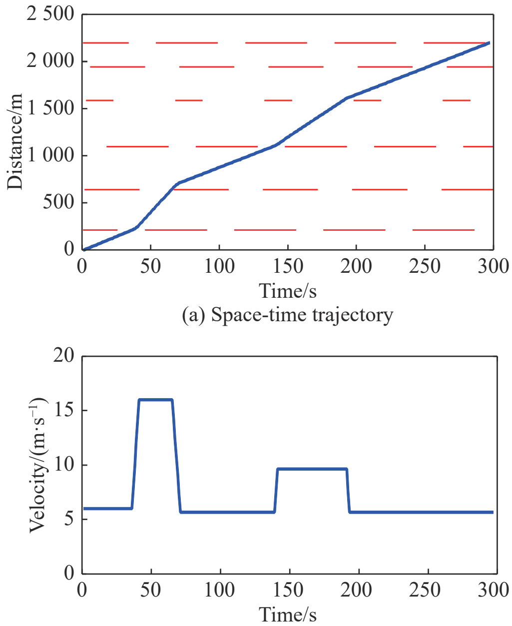

(a) Space-time trajectory

(b) Velocity

Fig. 8 Space-time trajectory and velocity of the CEV-BSS

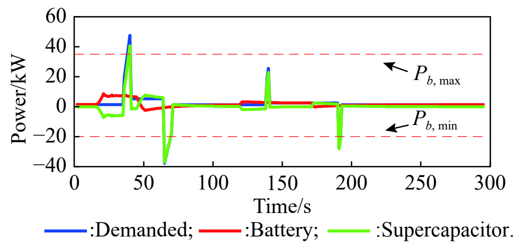

Fig. 9 Power-split results of the proposed strategy

Meanwhile, the SOC trajectories of battery and supercapacitor shown in Fig. 10 indicate that the proposed strategy ensures that the battery is not exhausted and supercapacitor SOC fluctuates around 75% at all times. This satisfies the terminal constraint in (15) and is beneficial to handle the upcoming unknown power demands in the future. Above all, the battery and supercapacitor operate within their allowable constraints.

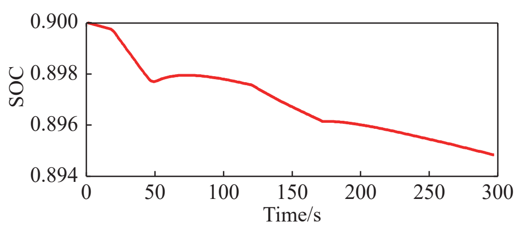

(a) Battery SOC

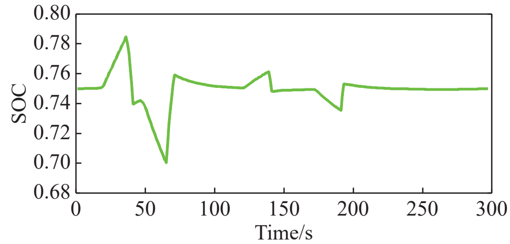

(b) Supercapacitor SOC

Fig. 10 Evaluation of SOC for the BSS

4.2 Comparison with hierarchical methods

In this subsection, a hierarchical method [29] with higher-level MPC and lower-level adaptive ECMS strategy is used as the baseline strategy to verify the comprehensive performance of the proposed strategy in terms of transportation efficiency, energy consumption, battery capacity loss and computing time. The simulation scenario is also introduced from [29], where the periods of the red/green signal light and the distance between adjacent signal lights are sampled from a uniform distribution with range 37−43 s/12−17 s and 300−500 m, respectively. Moreover, the initial signal light and vehicle velocity are also sampled from a uniform distribution with range 0−49 s and 6−12 m/s, respectively. The details are presented in Table 5.

Table 5 Details of simulation scenario

Signal light	Initial state/s	Interval (t_r/t_g)/s	Distance/m
1st	r-16	42/13	451
2nd	r-12	38/15	376
3rd	r-31	43/14	414
4th	g-14	39/14	315
5th	r-21	38/16	311

As shown in Fig. 11(a), even though both the proposed strategy and the baseline strategy can get through each intersection during the green light, the space-time trajectories indicate that the proposed strategy achieves shorter travel time compared with the baseline strategy, where the travel time for the proposed strategy is 138 s but 193 s for the baseline strategy. Meanwhile, it can be observed in Fig. 11(b) that the proposed strategy adopts a driving behavior that is completely different from the baseline strategy. Especially, at the first intersection, the proposed strategy speeds up the CEV-BSS to get through the intersection within the current green light owing to the fact that the L_1 regularization in (14) provides a sparse velocity for CEV-BSS.

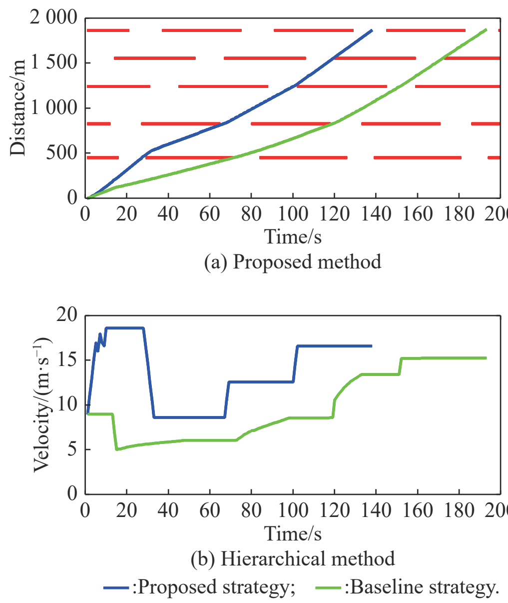

Fig. 11 Space-time trajectories and velocities based on the proposed and the hierarchical method

The power-split results are presented in Fig. 12. Obviously, although the baseline strategy achieves a lower peak of instantaneous demanded power for CEV-BSS at the cost of travel time, it leads to a worse power-split result compared with the proposed strategy since the higher-level controller of the baseline strategy does not consider the states of BSS when planning the velocities. Moreover, Fig. 13 illustrates that the proposed strategy is able to efficiently reduce the accumulative current throughput of battery. It means that the battery life can be prolonged because the battery capacity loss is heavily related with the ampere-hour throughput of battery. Since the lifecycle of supercapacitor is 100 times that of battery before battery capacity is lower than 80% of its nominal capacity [37], the capacity loss of supercapacitor is not considered in this paper.

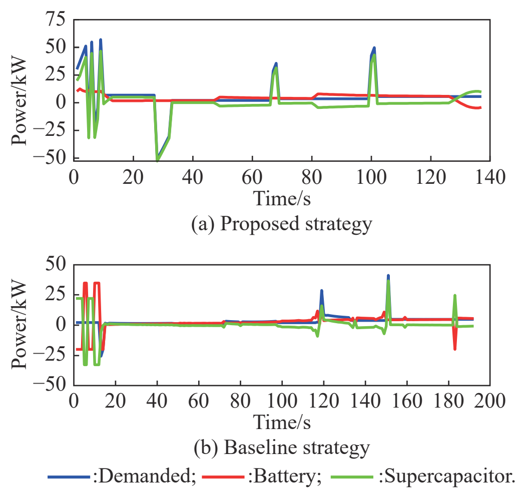

Fig. 12 Power-split results for the proposed strategy and the baseline strategy

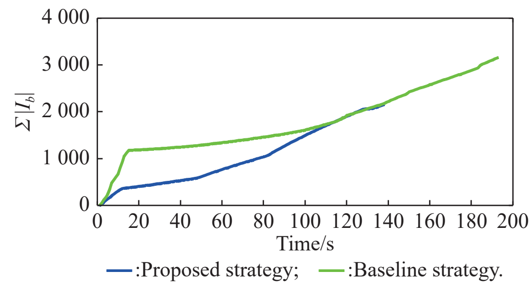

Fig. 13 Accumulative current throughput of battery $\Sigma|\boldsymbol{I}_b|$ for the proposed and baseline strategy

In order to evaluate the adaptive capability of the strategies with respect to the various urban traffic scenes, four scenarios separately considering 5, 10, 15 and 20 signal lights, denoted by L05, L10, L15 and L20, are employed in the simulation in the subsection. All simulation experiments are performed on a laptop with a 1.7 GHz CPU and 8 G memory. The statistical results are summarized in Tables 6–9 including travel time, accumulative current throughput of battery $\Sigma|I_b|$, final SOC of battery, and average CPU time.

Table 6 Travel time for proposed and baseline strategies

Scenario	Travel time/s		Improvement/%
	Proposed	Baseline	
L05	138	193	29
L10	388	482	20
L15	639	791	19
L20	887	1 050	16

Table 7 Accumulative current throughput of battery

Scenario	Accumulative current throughput/mA		Improvement/%
	Proposed	Baseline	
L05	2.1545	3.1636	68
L10	3.4135	9.9033	34
L15	5.9290	21.234	28
L20	7.5566	25.553	30

Table 8 Final SOC of battery %

Scenario	Final SOC		Improvement
	Proposed	Baseline	
L05	89.39	89.40	−0.01
L10	89.09	89.07	0.02
L15	88.40	88.28	0.12
L20	87.90	87.55	0.35

Table 9 Average CPU time ms

Scenario	Proposed	Baseline	
		High level	Low level
L05	188.0	456.4	87.0
L10	163.8	450.8	89.2
L15	144.5	450.2	117.1
L20	145.5	473.1	121.2

The travel time in Table 6 indicates that the proposed strategy can effectively reduce travel time for CEV-BSS and improve transportation efficiency by at least 16% under the same scenarios compared with the baseline strategy.

Meanwhile, it can be observed from Table 7 that the proposed strategy is able to cut down approximately 30% current throughput of battery compared to the baseline strategy when the driving distance increases. Generally, since the capacity of supercapacitor is far less than that of battery, only the difference of final SOC of battery between different strategies is discussed.

In Table 8, the index of 'Final SOC of battery' represents the total power consumption over the trips. From Table 8, one can see that the lower the final SOC is, the more power is consumed. In Scenario L05, although the Final SOC index of the proposed strategy is slightly worse than that of the baseline strategy, it can be seen from Table 6 and Table 7 that the corresponding 'Travel time' and 'Accumulative current throughput' are improved by 29% and 68%, respectively. This phenomenon implies that the proposed strategy can improve the traffic efficiency and prolong battery life-time under the same electric energy consumption. From Tables 6–8, one can further find that the proposed strategy can improve the traffic efficiency and prolong battery life-time with the lower electric energy consumption for Scenarios L10, L15 and L20. These verify the better adaptive capability to unknown scenarios of the monolayer MPC than that of hierarchical MPC.

Furthermore, the performance of real-time optimization is also an important index for evaluating the power-split strategy. As the average CPU time shown in Table 9, the proposed strategy has an almost three-fold improvement in computational efficiency compared with the higher-level controller of the baseline strategy.

5. Conclusions

In this paper, a flexible predictive power-split control strategy is proposed for CEV-BSS to improve transportation efficiency, reduce energy consumption and relieve battery degradation. The simulation results based on real-world scenarios reveal that the proposed strategy enables the CEV-BSS to get through each intersection at a gentle velocity during the green light and achieves a lower-level output power for battery. Furthermore, the comparisons of the proposed method with a hierarchical method indicate that the proposed method is able to improve transport efficiency by at least 16%, cut down nearly 30% current throughput of battery, reduce nearly 0.4% energy consumption and enhance almost three-fold computational efficiency. In the future work, the scenarios of multiple CEV-BSS, and even the traffic jam scenario are worthy to study in the context of traffic control [40]. Moreover, theoretical analysis of the feasibility, stability and robustness issues of the proposed PMP based nonlinear MPC will be further pursued to be studied.

References

[1] LIAN R Z, PENG J K, WU Y K, et al. Rule-interposing deep reinforcement learning based energy management strategy for power-split hybrid electric vehicle. Energy, 2020, 197: 117297.

[2] CAO J, ALI E. A new battery/ultracapacitor hybrid energy storage system for electric, hybrid, and plug-in hybrid electric vehicles. IEEE Trans. on Power Electronics, 2012, 27(1): 122–132.

[3] SONG Z Y, LI J Q, HAN X B, et al. Multi-objective optimization of a semi-active battery/supercapacitor energy storage system for electric vehicles. Applied Energy, 2014, 135: 212–224.

[4] CHUNG C H, JANGRA S, LAI Q Z, et al. Optimization of electric vehicle charging for battery maintenance and degradation management. IEEE Trans. on Transportation Electrification, 2020, 6(3): 958–969.

[5] ZHANG Q, DENG W E, LI G. Stochastic control of predictive power management for battery/supercapacitor hybrid energy storage systems of electric vehicles. IEEE Trans. on Industrial Informatics, 2018, 14(7): 3023–3030.

[6] NGUYEN B H, GERMAN R, JOAO P F, et al. Real-time energy management of battery/supercapacitor electric vehicles based on an adaptation of Pontryagin's minimum principle. IEEE Trans. on Vehicular Technology, 2019, 68(1): 203–212.

[7] ABODULLAH A M, LIU Z F, RIZZO D M, et al. An integrated design and control optimization framework for hybrid military vehicle using lithium-ion battery and supercapacitor as energy storage devices. IEEE Trans. on Transportation Electrification, 2019, 5(1): 239–251.

[8] SHEN J Y, KHALIGH A. Design and real-time controller implementation for a battery-ultracapacitor hybrid energy storage system. IEEE Trans. on Industrial Informatics, 2016, 12(5): 1910–1918.

[9] DUSMEZ S, KHALIGH A. A supervisory power-splitting approach for a new ultra-capacitor-battery vehicle deploying two propulsion machines. IEEE Trans. on Industrial Informatics, 2014, 10(3): 1960–1971.

[10] CHEN Z, MI C C, XIA B, et al. Energy management of power-split plug-in hybrid electric vehicles based on simulated annealing and Pontryagin's minimum principle. Journal of Power Sources, 2014, 272: 160–168.

[11] SUN H C, FU Z M, TAO F Z, et al. Data-driven reinforcement-learning-based hierarchical energy management strategy for fuel cell/battery/ultracapacitor hybrid electric vehicles. Journal of Power Sources, 2020, 455: 227964.

[12] TRAN D D, MAJID V, BAGHDADI M E, et al. Thorough state-of-the-art analysis of electric and hybrid vehicle powertrains: topologies and integrated energy management strategies. Renewable and Sustainable Energy Reviews, 2020, 119: 109596.

[13] QU X B, YU Y, ZHOU M F, et al. Jointly dampening traffic oscillations and improving energy consumption with electric,

connected and automated vehicles: a reinforcement learning based approach. Applied Energy, 2020, 257: 114030.
[14] XU F G, SHEN T L. Look-ahead prediction-based real-time optimal energy management for connected HEVs. IEEE Trans. on Vehicular Technology, 2020, 63(3): 2537–2551.
[15] GONG X, WANG J Y, MA B L, et al. Real-time integrated power and thermal management of connected HEVs based on hierarchical model predictive control. IEEE/ASME Trans. on Mechatronics, 2021, 26(3): 1271–1282.
[16] YAO Z H, ZHAO B, YUAN T F, et al. Reducing gasoline consumption in mixed connected automated vehicles environment: a joint optimization framework for traffic signals and vehicle trajectory. Journal of Cleaner Production, 2020, 265: 121836.
[17] WU J L, ZOU Y, ZHANG X D, et al. A hierarchical energy management for hybrid electric tracked vehicle considering velocity planning with pseudospectral method. IEEE Trans. on Transportation Electrification, 2020, 6(2): 703–716.
[18] GUO L L, GAO B Z, CHEN H. Optimal energy management for HEVs in eco-driving applications using bi-level MPC. IEEE Trans. on Intelligent Transportation Systems, 2017, 18(8): 2153–2162.
[19] ZHAO L H, MAHBUB A M, ANDREAS A M. Optimal vehicle dynamics and powertrain control for connected and automated vehicles. Proc. of the Conference on Control Technology and Applications, 2019: 33–38.
[20] XIE S B, QI S W, LANG K, et al. Coordinated management of connected plug-in hybrid electric buses for energy saving, inter-vehicle safety, and battery health. Applied Energy, 2020, 268: 115028.
[21] SANGJAE B, YEOJUN K, GUANETTI J, et al. Design and implementation of ecological adaptive cruise control for autonomous driving with communication to traffic lights. Proc. of the American Control Conference, 2019: 33–38.
[22] YE F, HAO P, QI X W, et al. Prediction-based eco-approach and departure at signalized intersections with speed forecasting on preceding vehicles. IEEE Trans. on Intelligent Transportation Systems, 2019, 20(4): 1378–1389.
[23] YUAN J N, YANG L. Predictive energy management strategy for connected 48V hybrid electric vehicles. Energy, 2019, 187: 115952.
[24] HE X Z, WU X K. Eco-driving advisory strategies for a platoon of mixed gasoline and electric vehicles in a connected vehicle system. Transportation Research Part D: Transport and Environment, 2018, 63: 907–922.
[25] HE D F, WANG L, SUN J. On stability of multiobjective NMPC with objective prioritization. Automatica, 2015, 57: 189–198.
[26] QIU L H, QIAN L J, ZOMORODI H, et al. Global optimal energy management control strategies for connected four-wheel-drive hybrid electric vehicles. IET Intelligent Transportation Systems, 2017, 11(5): 264–272.
[27] YU K J, YANG J Q, DAISUKE Y. Model predictive control for hybrid vehicle ecological driving using traffic signal and road slope information. Control Theory Technology, 2015, 13(1): 17–28.
[28] HE D F, SHI Y J, LI H P, et al. Multi-objective predictive cruise control for connected vehicle systems on urban conditions with InPA-SQP. Optimal Control Applications and Methods, 2019, 40(3): 479–498.
[29] BAISRAVAN H, LIN R N, PISU P. Hierarchical control strategies for energy management of connected hybrid electric vehicles in urban roads. Transportation Research Part C: Emerging Technologies, 2016, 62: 70–86.
[30] HUANG Y J, WANG H, AMIR K, et al. Model predictive control power management strategies for HEVs: a review. Journal of Power Sources, 2017, 341: 91–106.
[31] YU S M, LIN D, SUN Z, et al. Efficient model predictive control for real-time energy optimization of battery-supercapacitors in electric vehicles. International Journal of Energy Research, 2020, 44(9): 7495–7506.
[32] ZHENG C H, LI W, LIANG Q. An energy management strategy of hybrid energy storage systems for electric vehicle applications. IEEE Trans. on Sustainable Energy, 2018, 9(4): 1880–1888.
[33] ZHANG F Q, HU X S, LANGRAI R, et al. Energy management strategies of connected HEVs and PHEVs: recent progress and outlook. Progress in Energy and Combustion Science, 2019, 73: 235–256.
[34] ATKINSON C, LEWIS A, SALVIA A, et al. Powertrain innovations for connected and autonomous vehicles. Proc. of the Powertrain Innovation Workshop, 2015: 1–8.
[35] KAMAL M A S, MUKAI M, MURATA J, et al. Model predictive control of vehicles on urban roads for improved fuel economy. IEEE Trans. on Control Systems Technology, 2013, 21(3): 831–841.
[36] JING W L, LAI C H, WONG S H W, et al. Battery-supercapacitor hybrid energy storage system in standalone DC microgrids: a review. IET Renewable Power Generation, 2017, 11(4): 461–469.
[37] GOLCHOUBIAN P, AZAD N L. Real- time nonlinear model predictive control of a battery-supercapacitor hybrid energy storage system in electric vehicles. IEEE Trans. on Vehicular Technology, 2017, 66(11): 9678–9688.
[38] CANNON M, LIAO W H, BASIL K. Efficient MPC optimization using Pontryagin's minimum principle. Proc. of the 45th Conference on Decision and Control, 2006: 5459–5464.
[39] XIE S B, HU X S, XIN Z K, et al. Pontryagin's minimum principle based model predictive control of energy management for a plug-in hybrid electric bus. Applied Energy, 2019, 236: 893–905.
[40] CICIC M, XIONG X, JIN L, et al. Coordinating vehicle platoons for highway bottleneck decongestion and throughput improvement. IEEE Trans. on Intelligent Transportation Systems, 2022, 23(7): 8959–8971.

Biographies

HE Defeng was born in 1979. He received his bachelor's degree in thermal energy and power engineering from Central South University, Changsha, China, in 2001 and doctorate degree in control science and engineering from University of Science and Technology of China, Hefei, China, in 2008. Since 2015, he has been a full professor at Zhejiang University of Technology, Hangzhou, China. He has been the author of more than 100 research publications and has authorized more than 30 Chinese invention patents. His research interests include intelligent prediction and optimal control of autonomous systems.

E-mail: hdfzj@zjut.edu.cn

LUO Jie was born in 1997. He received his B.S. degree in automation from Zhejiang University of Technology, Hangzhou, China, in 2019. He is currently pursuing his Ph.D. degree in control science and engineering from Zhejiang University of Technology, Hangzhou, China. His research interests include model predictive control and its applications to connected and automated vehicles.

E-mail: 2111903059@zjut.edu.cn

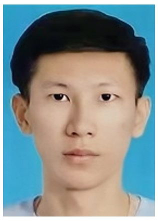

LIN Di was born in 1993. He received his M.S. degree in control science and engineering from Zhejiang University of Technology, Hangzhou, China, in 2021. He is currently a full engineer at the BYD Company Limited, Huizhou, China. His research interests include model predictive control and its applications to connected and automated vehicles.

E-mail: 2111803060@zjut.edu.cn

YU Shiming was born in 1962. He received his Ph.D. degree in control theory and control engineering from Zhejiang University, Hangzhou, China, in 2001. He is currently a full professor at Zhejiang University of Technology, Hangzhou, China. His research interests include model predictive control and system identification.

E-mail: ysm@zjut.edu.cn